OPEN

Light: Science & Applications (2014) 3, e185; doi:10.1038/lsa.2014.66

www.nature.com/lsa

ORIGINAL ARTICLE

Design and fabrication of broadband ultralow reflectivity black Si surfaces by laser micro/nanoprocessing

Jing Yang[1,2,3,*], Fangfang Luo[1,*], Tsung Sheng Kao[1], Xiong Li[4], Ghim Wei Ho[1], Jinghua Teng[2], Xiangang Luo[4] and Minghui Hong[1]

Light collection efficiency is an important factor that affects the performance of many optical and optoelectronic devices. In these devices, the high reflectivity of interfaces can hinder efficient light collection. To minimize unwanted reflection, anti-reflection surfaces can be fabricated by micro/nanopatterning. In this paper, we investigate the fabrication of broadband anti-reflection Si surfaces by laser micro/nanoprocessing. Laser direct writing is applied to create microstructures on Si surfaces that reduce light reflection by light trapping. In addition, laser interference lithography and metal assisted chemical etching are adopted to fabricate the Si nanowire arrays. The anti-reflection performance is greatly improved by the high aspect ratio subwavelength structures, which create gradients of refractive index from the ambient air to the substrate. Furthermore, by decoration of the Si nanowires with metallic nanoparticles, surface plasmon resonance can be used to further control the broadband reflections, reducing the reflection to below 1.0% across from 300 to 1200 nm. An average reflection of 0.8% is achieved.
Light: Science & Applications (2014) **3,** e185; doi:10.1038/lsa.2014.66; published online 4 July 2014

Keywords: anti-reflection; broadband; laser micro/nanoprocessing; surface plasmons

INTRODUCTION

Natural optical systems, such as the eyes of various animals, are capable of visualizing a wide spectrum of colors. Nature can serve as an inspiration to scientists attempting to design better optical systems, leading to the development of biomimetic systems.[1] Biomimetic anti-reflection systems are one example of this approach. The surface of a moth's eye has unique subwavelength structures that can dramatically reduce light reflection, helping the moth to improve light collection in the dark and avoid predators in the light. Various optical devices are designed in similar ways to enhance anti-reflection performance. When light, i.e., intrinsically electromagnetic waves, enters a different media, it is partially reflected due to refractive index (RI) mismatching. In various optical and optoelectronic devices, including flat panel displays, photovoltaic devices and optical detectors,[1–11] reflections at interfaces can greatly impact performance. To minimize unwanted reflections and improve the light collection efficiency, different types of anti-reflection surfaces have been investigated.[1–3,5,8,12–16]

Si is one of the most important materials in optical and optoelectronic devices.[14] Light absorption by Si occurs below ~1100 nm, corresponding to the single crystalline Si energy band gap. However, between 300 and 1200 nm, the light collection efficiency of a Si surface is not sufficiently high for many applications due to the relatively high reflectivity at the air/Si interface caused by the large RI of Si.[14,15,17] Thus, anti-reflection black Si surfaces are of widespread interests.

Recent advances in surface micro/nanofabrication and thin film deposition have provided versatile approaches for decorating Si surfaces with engineered structures that can reduce optical reflections. For example, deposit of a single layer thin film with specially designed RI and thickness on a Si substrate can serve as an anti-reflection coating.[1,18] According to the Fresnel equation, the RI of the film is at normal incidence, while the thickness is an odd multiple of $\lambda/4$, where λ is the wavelength of the incident light and n_{air} and n_s are the RI of the air and Si substrate, respectively.[1] The reflection is minimized by the destructive interference between the reflected waves at the interfaces. Furthermore, multilayer thin film coatings are used to broaden the wavelength range for anti-reflection. With the appropriate design of the thickness and RI in each layer, sufficiently high anti-reflection performance can be achieved for broadband applications.

However, there are several limitations, including the small working angle and the mismatch in thermal properties of different materials that restrict the use of this method for certain applications. Textured Si surface, on the other hand, bypasses these limitations and provides better omnidirectional and broadband anti-reflection.[2,13–15,17–21] Textured Si surfaces with engineered micro/nanostructures can greatly enhance the light trapping effect, increasing the optical absorption and thereby reducing the surface reflection. The anti-reflection performance can be further improved by the use of subwavelength structures that form RI gradients. The effective RI depends on the volume fraction of Si and air for compensating the RI mismatch at

[1]Department of Electrical and Computer Engineering, National University of Singapore, Singapore 117576, Singapore; [2]Institute of Materials Research and Engineering, Agency for Science, Technology and Research, Singapore 117602, Singapore; [3]NUS Environmental Research Institute, National University of Singapore, Singapore 117411, Singapore and [4]State Key Laboratory of Optical Technologies for Microfabrication, Institute of Optics and Electronics, Chinese Academy of Sciences, Chengdu 610209, China
*These authors contributed equally to this work
Correspondence: Professor MH Hong, Department of Electrical and Computer Engineering, National University of Singapore, 4 Engineering Drive 3, Singapore 117576, Singapore
E-mail: elehmh@nus.edu.sg
Received 30 October 2013; revised 10 April 2014; accepted 12 April 2014

the interface.[22,23] There are several processing methods available for modifying the Si surface morphology.[1,5,7,13–15,17,19,24,25] For example, etching methods, including chemical, electrochemical and dry etching, have been widely employed.[26,27] Dynamic etching of porous Si surfaces to a thickness of 100 nm has been demonstrated by Striemer and Fauchet,[27] who achieved an average reflection of 3.7% across the terrestrial solar spectrum. Laser ablation provides another dry processing route for fabricating anti-reflection Si surfaces.[14,15,17,19] Black Si surfaces fabricated by short pulse lasers were studied by Mazur *et al.*[17] Conical shape surfaces structures can be created by laser processing. A recent review summarized this work and its application in photovoltaic cells.[28] Black Si surfaces directly fabricated by femtosecond laser irradiation were also demonstrated by Vorobyev and Guo.[15] In their report, the reflection of the black surface was below 5% over the visible spectrum. Subwavelength structures especially silicon nanowires (SiNWs) are also widely studied to achieve high light absorption in the visible and NIR range.[26,29,30] Kumar *et al.*[29] fabricated SiNW arrays and applied them to solar cells. The maximum reflection of their black Si surface was approximately 4% between 300 and 1000 nm. However, the reflection increased to more than 10% at longer wavelength range. Subwavelength structures, e.g., hybrid moth-eye structures[23] and ZnO coated Si nanocones,[18] have been numerically simulated to exhibit ultralow reflection. The theoretical solution for a graded index anti-reflection design has been studied in detail by Kim and Park.[22] They demonstrated ultrathin anti-reflection metamaterials and provided a design guideline for perfect broadband anti-reflection. Ding *et al.*[31] demonstrated perfect broadband anti-reflection on Si in the terahertz range by impedance matching by way of deep subwavelength ultrathin lamellar metallic gratings.

Another method worth mentioning for anti-reflection is the use of surface plasmon resonance (SPR) supported by metallic nanoparticles (NPs). With electromagnetic wave excitation, metallic NPs can be used as anti-reflection surfaces because they excite localized SPR that increases the optical absorption by light trapping.[2–5,13,32] The localized electromagnetic field around the metallic NPs can be significantly enhanced at their resonant frequencies.[33] In addition, the light scattering properties become dominant for larger NPs. Both of these effects contribute to the anti-reflection performance. Generally, Au and Ag NPs are used for SPR excitation in the visible range. To reduce the material cost, other metallic NPs, such as Al and Cu, have been investigated. However, these materials are more suitable for applications in the ultraviolet (UV) and infrared (IR) ranges given their SPR frequencies.[4,32] To reduce optical reflection over broadband, alloy NPs, such as Ag–Au NPs, have been applied.[5,13] Recently, Al and Ag NPs and their nanoshells were applied in Si solar cells by Gu *et al.*[2–4] The emergence of metallic NPs in addition to conventional anti-reflection surfaces can further improve the overall anti-reflection performance to increase the efficiency of optoelectronic devices.

In this article, we report our recent research on broadband ultralow reflectivity black Si surfaces fabricated by laser micro/nanoprocessing. Our laser processing method is able to create surface patterns over a large area in a short time, providing a cost effective solution for fabricating broadband anti-reflection surfaces.[34] We demonstrate high anti-reflection performance for our laser textured Si surfaces with micro/nanostructures. We also describe how the performance can be enhanced by the addition of metallic NPs that reduce optical reflection on flat Si surfaces. Finally, we integrate the laser micro/nanoprocessing and metallic NPs decoration method to realize broadband anti-reflection on Si surfaces. We achieve a reflection of less than 1.0% from 300 to 1200 nm.

ANTI-REFLECTION PERFORMANCE OF SI SURFACES BY LASER MICROPROCESSING

Roughened surfaces can reduce the optical reflection by light trapping. In this section, Si surfaces textured by laser-based methods are introduced. The conventional anti-reflection surface fabricated by KOH wet etching is indicated in Figure 1a as a reference.[13] To fabricate micropyramid structures on the Si surfaces, the n-type Si (100) substrates were first etched by HF (4%) to remove the oxide layer. The wafers were then immersed in a solution of KOH (6 wt%) and isopropyl alcohol (20%) at 70 ℃ for 30 min. The resulting micropyramids were 5–15 μm wide and approximately 2–8 μm tall. The aspect ratio (height/width) of the microstructures was ~1∶2. Figure 1b illustrates the experimental reflection spectra of a flat Si surface and a Si surface etched by KOH. The average reflection of the Si surface was reduced from 37.8% to 13.1% at 300–1200 nm by KOH etching. The maximum reflection was reduced from 56.6% to 33.1% at 300 nm. In contrast to the flat Si surface, the etched Si surface had numerous micropyramids, which redirected the incident light inside the Si substrate. For these surfaces, the incident light bounces from one micropyramid to another. This multiinternal reflection process can greatly increase the optical length of the incident light. Therefore, the opportunity for light absorption by the Si substrate is greatly enhanced.

Though the KOH-etched surfaces reduce reflections at the interface, the KOH wet etching cannot provide surface structures with high

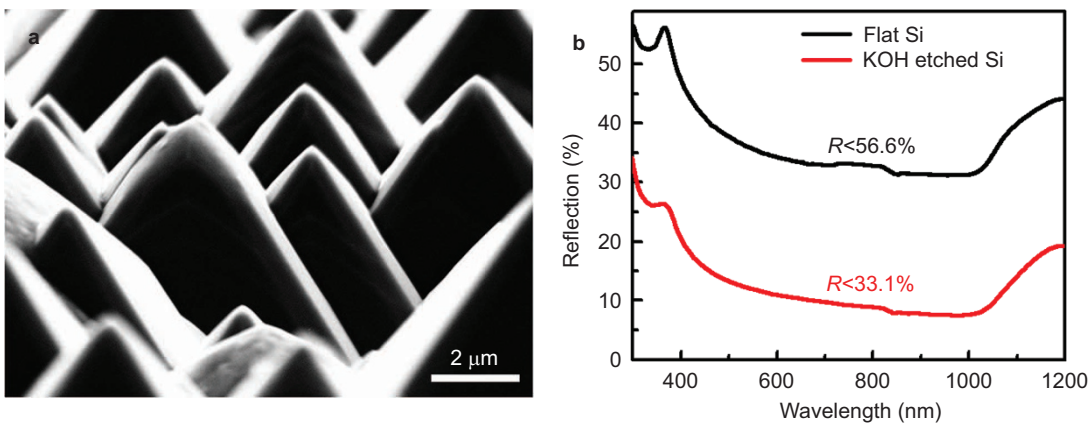

Figure 1 (**a**) SEM image of KOH etched Si surface and (**b**) measured reflection spectra of flat and KOH etched Si surfaces. SEM, scanning electron microscopy.

doi:10.1038/lsa.2014.66

enough aspect ratios, which limits the anti-reflection performance. Laser direct writing provides another method to texture Si surfaces with higher aspect ratio microstructures to enhance light trapping. A fiber laser ablation system was used to fabricate black Si (Figure 2a). The laser wavelength was 1064 nm, the pulse duration (full width at half maximum) was 1 ns and the laser spot size was ~20 μm. This method was able to create microstructures on the Si substrates over a large area of 10×10 cm^2 in only a couple of minutes, as shown in Figure 2b and 2c. Compared to the KOH wet etching, the laser ablation created surface structures with higher aspect ratios, which is a key factor for better light trapping. Figure 2d shows the surface profile of the laser textured Si surface. The height of the surface structures exceeded 15 μm, with width at ~10 μm and an aspect ratio of ~3 : 2. To optimize the anti-reflection performance, the different processing parameters for the laser ablation, including the power, pulse repetition rate (PRR), scanning pitch and scanning speed, were tuned. Hybrid Laser patterning, which produces different scanning patterns along different directions, was adopted for surface texturing. The patterns were generated by laser scanning along the horizontal, vertical, +45° and −45° directions.

Figure 3a shows the experimental reflection spectra of the laser textured Si surfaces at different laser powers. Hybrid laser patterning was adopted in the experiment. As the power increased from 2.3 to 4.2 W, the reflection decreased for wavelengths ranging from 300 to 1200 nm because at a higher laser power, more intense ablation leads to the removal of more substrate material. Thus, the roughness of the Si surface increases as does the aspect ratio, resulting in less optical reflection. Figure 3b illustrates the reflection spectra of the textured Si surfaces at different scanning pitches. To properly study the influence of the scanning pitch, laser patterning was carried out only along the horizontal direction. It was observed that a smaller pitch led to a lower reflection. For a smaller pitch, the density of the microstructures and the surface area are greater, resulting in more opportunities for light trapping and absorption. The effects of the PRR and scanning speed were also studied, as shown in Figure 3c and 3d. Generally speaking, a lower scanning speed and a higher PRR result in better anti-reflection performance. The Δl is defined as the center to center distance of two spots ablated by neighboring pulses. It is given by $\Delta l = \frac{v}{\mathrm{PRR}}$, where v is the scanning speed. Either a decrease in laser scanning speed or an increase in PRR will result in a smaller Δl. With the same laser power and spot size, the ablation area of each pulse is the same. Therefore, a smaller Δl increases the overlap during the laser ablation. Thus, the roughness of the Si surface increases, reducing the optical reflection. In our experiment, broadband surface reflections below 14.3% were achieved by fiber laser ablation at 4.2 W, with a 100 mm s^{-1} scanning speed, 100 kHz PRR and 25 μm scanning pitch. In this case, the average reflection was 7.4%. We were also able to fabricate microstructures on 4-inch ultrathin Si substrates by laser ablation. At a thickness of 100 μm, the black Si can be easily bent. These flexible substrates can be more easily integrated with other optical devices to reduce the surface

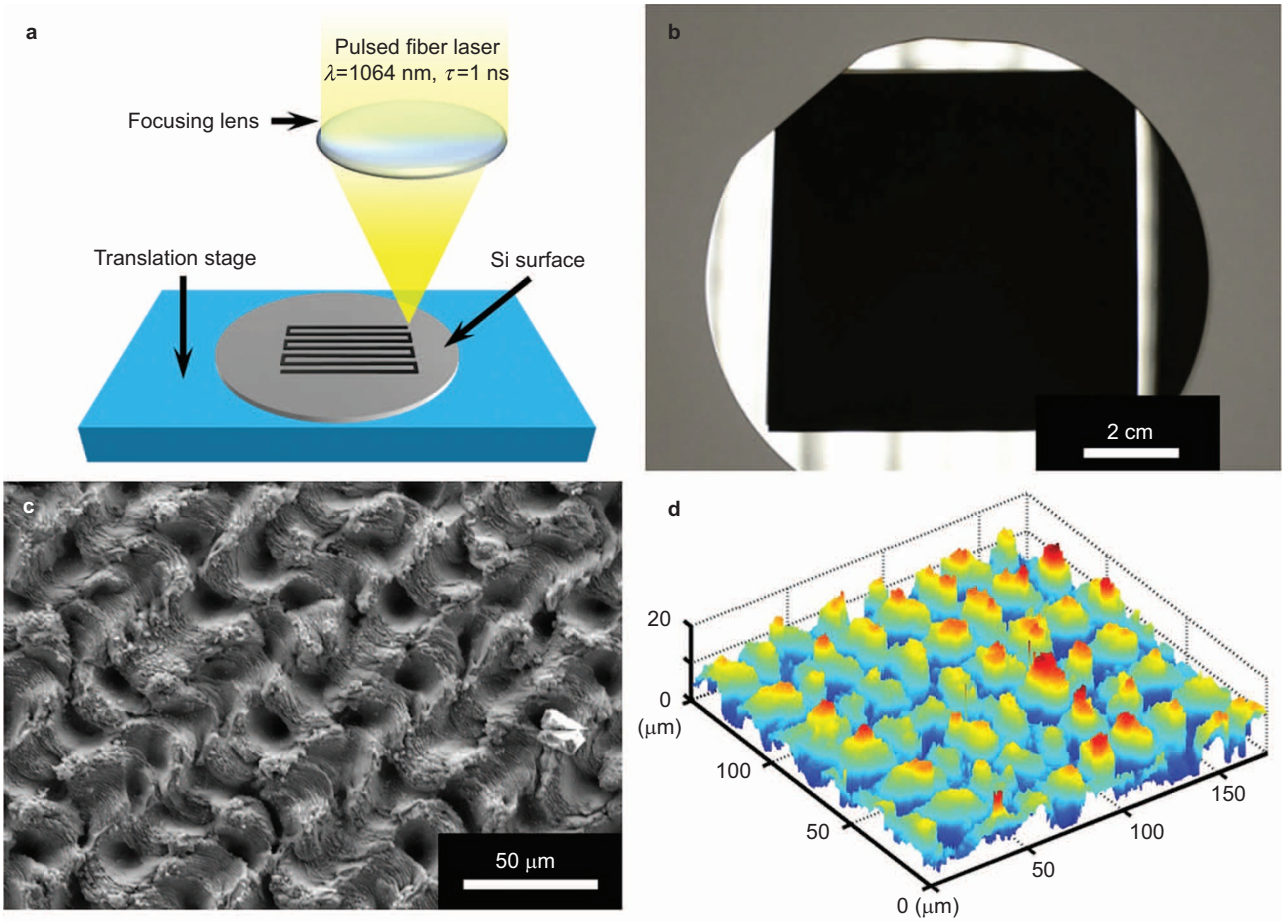

Figure 2 (**a**) Schematic of fiber laser ablation for black Si surface fabrication, (**b**) image of the textured black Si surface, its (**c**) SEM image and (**d**) 3D surface profile. 3D, three-dimensional; SEM, scanning electron microscopy.

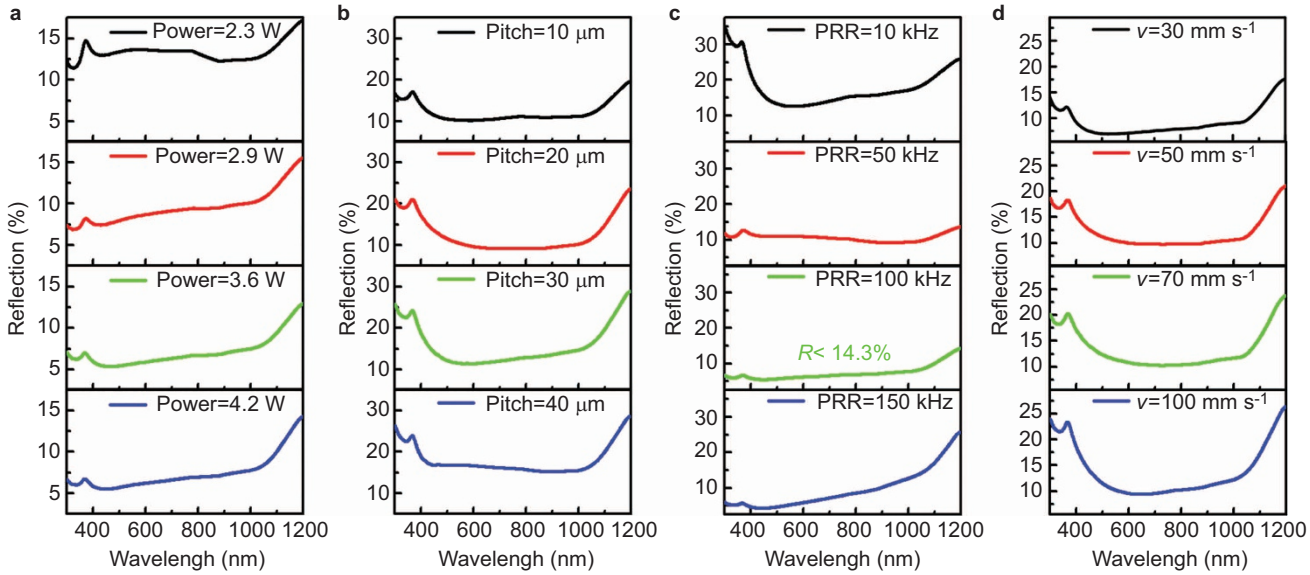

Figure 3 Reflection spectra of black Si surfaces textured by the fiber laser ablation at different laser: (**a**) powers, (**b**) pitches, (**c**) PRRs and (**d**) scanning speeds (*v*). The default laser power is 4.2 W, scanning pitch is 25 μm, PRR is 100 kHz and scanning speed is 100 mm s^{-1} (laser spot size: ~20 μm). PRR, pulse repetition rate.

reflection and increase the light collection efficiency. Similarly, a femtosecond laser can be used to fabricate black Si surfaces. It can create smaller surface structures with shorter pulse durations and reduced thermal effect. The increase in the surface aspect ratio of these structures leads to better anti-reflection performance.[14,15,17]

ANTI-REFLECTION PERFORMANCE OF SI SURFACES BY LASER NANOPROCESSING

The textured surface structures produced by laser ablation are on the micron-scale. The size and aspect ratio of the surface structures are limited by the laser processing parameters. Our theoretical simulations show that with much higher aspect ratios, surface nanostructures can provide a better solution for broadband anti-reflection.[18,23]

Laser interference lithography (experimental set-up is shown in Figure 4a) and metal assisted chemical etching were adopted to make three-dimensional (3D) SiNWs with high aspect ratios of up to 30∶1 over an area of 1×1 cm^2, as illustrated in Figure 4b. To fabricate the SiNW arrays, a positive photoresist S1805 was spin-coated on a flat Si substrate. The substrate was then baked at 90 ℃ for 15 min. The photoresist was exposed twice by laser interference lithography with a 90°rotation of the sample between the two rounds of exposure. After photoresist development, a layer of Ag (~30 nm thick) was deposited by e-beam evaporation (EB03, BOC Edwards). The substrate was then chemically etched in a solution of H_2O_2 (0.44 M), HF (4.6 M) and H_2O. The etching time was adjusted from 1 to 20 min to make SiNWs with heights ranging from 1 to 30 μm. The Ag film was then removed by nitric acid.

Figure 5a–5c shows scanning electron microscopy (SEM) images of SiNWs of different heights. The period of the SiNWs was ~720 nm and the diameter was ~300 nm. The SiNWs maintained good periodicity at heights from 1 to 9 μm. At a height of ~30 μm, the mechanical strength of the nanostructure could no longer support the nanowires. Several adjacent SiNWs were observed to lean together to form SiNW clusters, resulting in a loss of periodicity. Figure 5d shows the measured spectra for SiNWs of different heights. The reflection from the 1-μm SiNWs was approximately 10% at wavelengths ranging from 300 to 1000 nm. A sharp increase in the reflection of up to 32.0% was observed between 1000 and 1200 nm. The 1-μm SiNWs exhibited lower reflectivity (average reflection of 11.8% and broadband reflection below 32.0%) than the flat Si. However, compared to the laser ablation textured black Si, the anti-reflection performance was not improved. There are a few explanations for this result. First, the low aspect ratio (~3∶1) can limit the light trapping. The light absorption by the Si surface is weak, especially at 1000–1200 nm, which is close to the single crystalline Si band gap of 1100 nm. Thus, some of the light goes into the Si substrate and is reflected back from the back side. The flat surfaces at the sidewalls, top and bottom surfaces of the SiNWs also limit the light trapping.

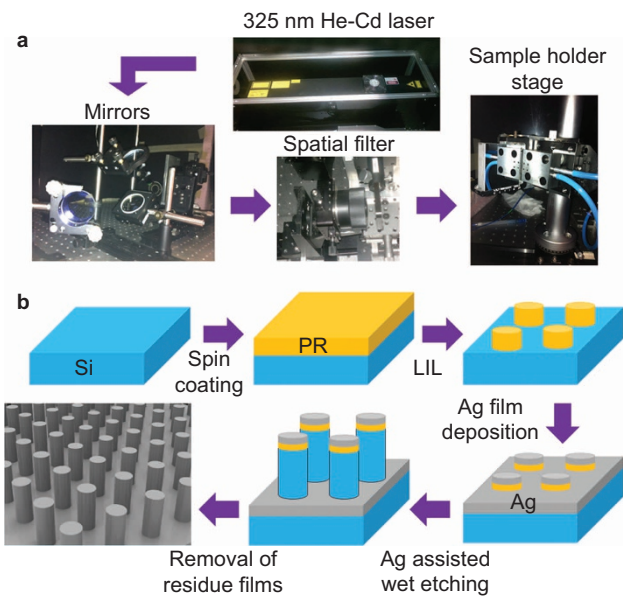

Figure 4 (**a**) Experimental set-up of laser interference lithography and (**b**) fabrication process for large-area 3D SiNW arrays. 3D, three-dimensional; LIL, laser interference lithography; PR, photoresist; SiNW, silicon nanowire.

doi:10.1038/lsa.2014.66

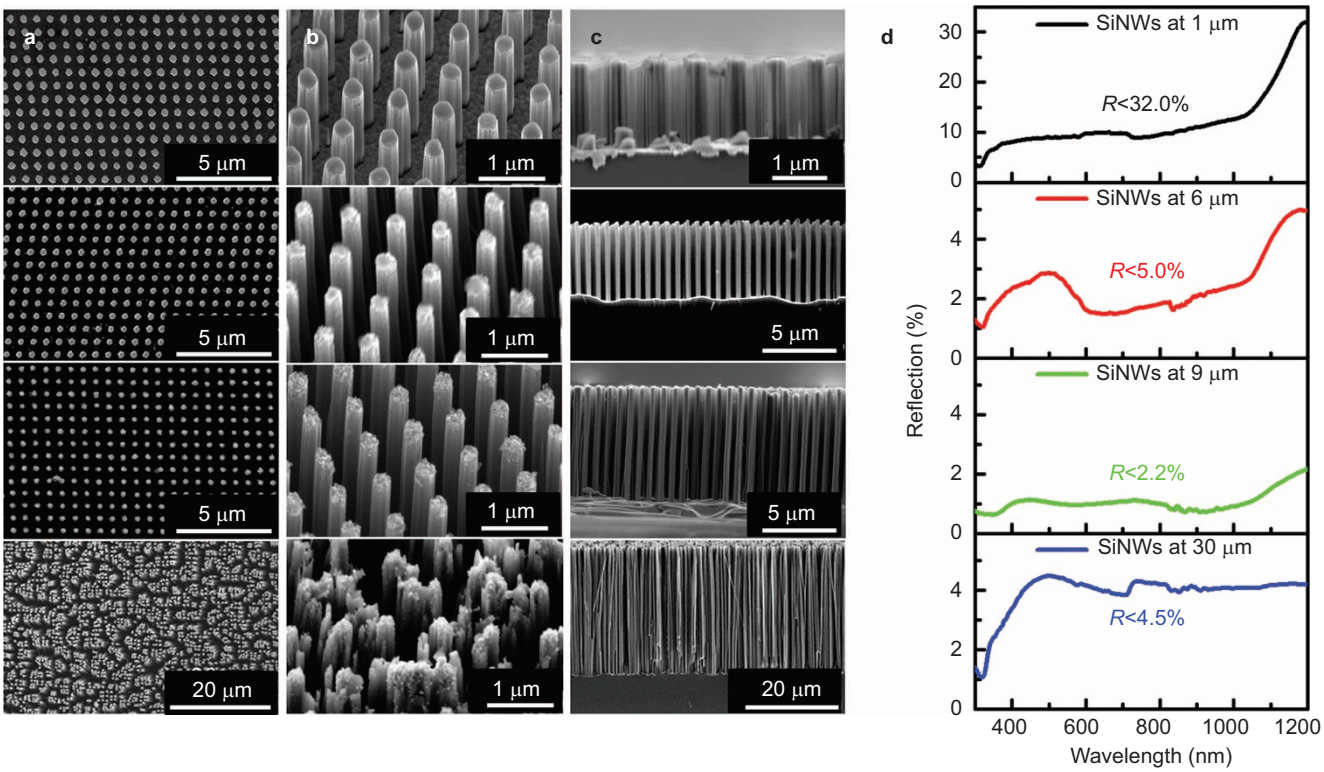

Figure 5 SEM images of SiNWs at different heights (period: ~720 nm, diameter: ~300 nm): (**a**) top-view, (**b**) tilt-view (35°), (**c**) side-view and (**d**) measured reflection spectra of the SiNWs at different heights. 3D, three-dimensional; SEM, scanning electron microscopy; SiNW, silicon nanowire.

Figure 5b shows that the surface profile at the top side of the 1-μm SiNWs is nearly identical to the original flat Si. It is much smoother than that of SiNWs at other heights due to the short etching time of 1 min. Though the top area of a single SiNW is small, the overall top area is large considering the high SiNW density. The flat tops of the SiNWs contribute to the high reflection of the surface.

As the SiNW height increases to 6 and 9 μm, the surface reflection decreases for 300 to 1200 nm light. The subwavelength SiNWs can be treated as an intermediate layer with an effective RI. The effective RI can be calculated by the volume fractions of Si and air. It can compensate for RI mismatching at Si/air interface, thus reducing the reflection at the Si/air interface. Meanwhile, the ultrahigh aspect ratio provides more opportunities for light trapping among the Si structures. The enlarged vertical dimension is more likely to trap the incident light by internal reflection. Moreover, compared to the 1 μm SiNWs, the top surfaces of the 6- and 9-μm-tall SiNW are rougher due to the longer etching time. Such rough surfaces also help to reduce the reflection. Therefore, at a height of 6 μm the broadband reflection from the SiNWs can be reduced to below 5.0%, achieving an average reflection of 2.4%. Furthermore, at a height of 9 μm the average reflection from the SiNWs is reduced to 1.1% with a broadband reflection below 2.2%. The maximum reflection at 2.2% is located at 1200 nm. The relatively high reflection in the infrared range is caused by the back side surface reflection of the Si substrate. When the height of the SiNWs is further increased to ~30 μm, SiNW clusters are generated. The light trapping effects are weakened due to the lower effective surface aspect ratio, leading to reduced light absorption. The overall anti-reflection performance (average reflection at 3.9% and broadband reflection below 4.5%) is weakened compared to SiNWs that are 6- and 9-μm tall.

ANTI-REFLECTION PERFORMANCE OF HYBRID ANTI-REFLECTION SURFACES

In addition to the surface texturing, SPR excitation is also considered to be an effective method for anti-reflection. Metallic NPs exhibit localized surface plasmon resonance (LSPR). The local field enhancement caused by LSPR can greatly influence the light absorption and scattering. Our previous study showed that both monometallic (Ag, Au) and bimetallic (Ag–Au) NPs significantly improve the anti-reflection performance.[5] Monometallic NPs can dramatically reduce the reflection in the visible range, while bimetallic NPs can enhance the anti-reflection performance over a wider spectrum. The improved broadband anti-reflection induced by bimetallic NPs is attributed to their multiple surface plasmon resonances. The broader size and shape distribution of bimetallic NPs leads to a broader SPR band for the antireflection. Meanwhile, the bimetallic NPs can roughen the surface morphology. A rougher surface will increase the light scattering and absorption. Therefore, bimetallic NPs exhibit much better broadband anti-reflection than monometallic NPs.

Textured Si surfaces and metallic NPs can reduce the reflection by different mechanisms. These two methods can also be combined together to fabricate hybrid surfaces with improved broadband anti-reflection performance.[13] To investigate the anti-reflection effect of metallic NPs, Ag, Ag–Au bimetallic and Cu–Ag–Au trimetallic NPs were decorated on Si surfaces by thermal annealing. Metallic thin films were first deposited on the Si surfaces by an e-beam evaporator. Thermal annealing at 200 ℃ (for Ag thin film) for 30 min or 500 ℃ (for Ag–Au and Cu–Ag–Au films) for 30 min was then carried out to decorate the Si surface with the metallic NPs.

Figure 6a shows an SEM image of a KOH-etched Si surface with Ag NPs decoration. The experimental reflection spectra for the

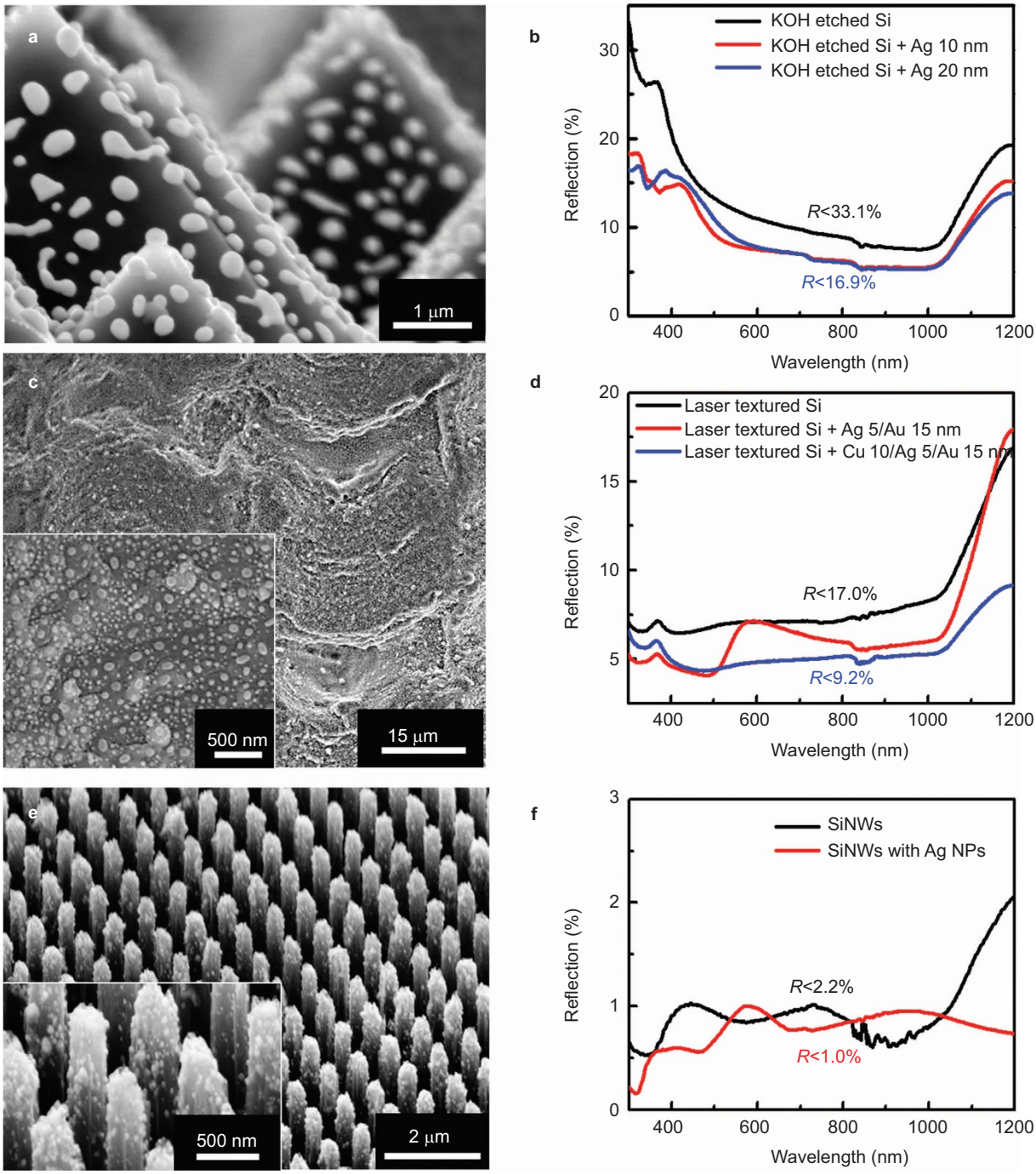

Figure 6 (**a**) SEM image of Ag NPs decoration of KOH etched Si surface and (**b**) measured reflection spectra of the KOH etched Si surfaces with and without Ag NPs decoration. (**c**) SEM images of the laser textured Si surfaces decorated with Ag–Au alloy NPs and (**d**) measured reflection spectra of laser textured Si surfaces with and without alloy NPs decoration. (**e**) SEM images of 3D SiNWs array decorated with Ag NPs and (**f**) measured reflection spectra of a 3D SiNWs array with and without Ag NPs decoration. 3D, three-dimensional; NP, nanoparticle; SEM, scanning electron microscopy; SiNW, silicon nanowire.

KOH-etched Si surfaces with and without Ag NPs are shown in Figure 6b. A dramatic suppression of the optical reflection was observed at wavelengths ranging from 300 to 400 nm. The Ag NPs created by thermal annealing of the 10 and 20 nm Ag thin films had similar suppression behaviors in terms of on the reflection spectra. The Ag NPs serve as an anti-reflection layer on the Si surface. The coupling of Ag NPs and the incident light is enhanced at their resonance wavelength of ~400 nm. Meanwhile, the textured Si surfaces extend the light propagation length as it travels among the micropyramids. This increases the chances of light absorption by the Ag NPs and the Si surfaces. The average reflection of the KOH-etched Si surface with Ag NPs (Ag 20) decoration was reduced to 9.2% at wavelengths ranging from 300 to 1200 nm. The maximum reflection of 16.9% occurred at 321 nm. Thus, the broadband reflection was below 16.9%.

Compared to the KOH-etched Si surface with Ag NPs decoration, the laser-textured black Si with alloy NPs decoration exhibited better

doi:10.1038/lsa.2014.66

Table 1 Anti-reflection performance of the different black Si surfaces

Type of anti-reflection surface	Average reflection from 300 to 1200 nm (%)	Maximum reflection from 300 to 1200 nm (%)
Flat Si	37.8	56.6
KOH etched Si	13.1	33.1
KOH etched Si + Ag 10 nm	9.2	18.3
KOH etched Si + Ag 20 nm	9.2	16.9
Laser textured Si	7.4	14.3
Laser textured Si + Ag 5/Au 15 nm	6.9	18.0
Laser textured Si + Cu 10/Ag 5/Au 15 nm	5.5	9.2
SiNWs at 1 μm	11.8	32.0
SiNWs at 6 μm	2.4	5.0
SiNWs at 9 μm	1.1	2.2
SiNWs at 30 μm	3.9	4.5
SiNWs at 9 μm + Ag 10 nm	0.8	1.0

Abbreviation: SiNW, silicon nanowire.

broadband anti-reflection performance.[13] Figure 6c shows an SEM image of the fiber laser-textured Si surface with Ag–Au bimetallic NPs decoration. The experimental reflection spectra of the fiber laser-textured Si surfaces with different alloy NPs decorations are illustrated in Figure 6d. The average reflection of the laser-textured Si surfaces was 8.3% at wavelengths ranging from 300 to 1200 nm, while the average reflection for the surfaces with Ag–Au and Cu–Ag–Au NPs decoration was reduced to 6.9% and 5.5%, respectively. It was observed that with Ag–Au bimetallic NPs decoration, the optical reflection at 300–500 nm decreased greatly due to the excitation of the LSPR. Meanwhile, the light scattering from the NPs-decorated Si surface also contributed to the anti-reflection performance. Compared to the Ag–Au bimetallic NPs decoration, the Cu–Ag–Au trimetallic NPs decoration more significantly suppressed the reflection, especially in the near Infrared range. This was due to the LSPR wavelength of the Cu NPs, which is also in the near infrared range. Thus, the trimetallic NPs decoration resulted in better broadband anti-reflection performance. The maximum reflection at 9.2% occurred at 1200 nm. Thus, a broadband reflection below 9.2% was achieved at 300–1200 nm.

To further improve the anti-reflection performance, a hybrid structure integrating SiNW arrays and metallic NPs was fabricated. Figure 6e shows the 9-μm SiNWs decorated with Ag NPs. The experimental reflection spectra of the SiNWs with and without NPs decoration are shown in Figure 6f. The SiNWs exhibited a higher aspect ratio of 30∶1, which provided a larger surface area for Ag NPs decoration. The increase in the density of Ag NPs contributed to the intensive coupling between the light and the NPs, which minimized the surface reflection. A drop in the reflection was observed at 400–500 nm. The decrease in reflection was mainly due to the enhanced light absorption by Ag NPs at their resonant frencies. Furthermore, in the near infrared range, the SiNWs with Ag NPs decorations exhibited better anti-reflection performance. Specifically, a significant suppression of reflection from 1000 to 1200 nm was observed. This was due to a reduction in the reflection from the backside Si surface. With greater light scattering by the Ag NPs, especially for the NPs-decorated at the sidewalls, and the top and bottom of the SiNWs, the opportunity for light scattering within the hybrid nanostructures increased. The incident and the backreflected light were thus more likely to be trapped inside the nanostructures, reducing the overall reflection. Meanwhile, the Ag NPs on the top of the SiNWs provided a rough surface that also reduced the surface reflection. As a result, the SiNWs with Ag NPs decoration flattened the reflection spectrum, providing a reflection below 1.0% from 300 to 1200 nm. The maximum reflection at 1.0% occurred at 572 nm. An average reflection of 0.8% was achieved.

Table 1 shows the anti-reflection performance of black Si surfaces fabricated by various processing methods. Significant suppression in the reflection spectra from 300 to 1200 nm can be observed using laser micro/nanoprocessing methods. The 9-μm-tall SiNWs decorated with Ag NPs exhibited the best broadband anti-reflection performance.

CONCLUSIONS

The last few decades have witnessed rapid progress in the design and fabrication of black Si surfaces. Realization of anti-reflection Si surfaces based on laser micro/nanoprocessing has enabled us to create surface patterns over large areas in a short time, providing a cost effective solution for broadband anti-reflection. We investigated textured Si surfaces with micro/nanostructures. Well-ordered SiNWs with high aspect ratios improved anti-reflection performance in the UV–visible–NIR range. Decoration of the Si with metallic NPs also reduced the surface reflection. Textured Si and metallic NPs have different mechanisms for reducing the optical reflection. We combined these two methods to fabricate hybrid surfaces that further improved the broadband anti-reflection. The SiNWs decorated with Ag NPs exhibited broadband ultralow reflection. Our black Si surfaces achieved reflections less than 1.0% over a wavelength range from 300 to 1200 nm. SiNW-based rough Si surfaces fabricated by conventional solar cell fabrication protocol,[35] including surface passivation and back surface field forming,[29,30] have been developed for solar cell integration. Similar approaches can be applied to our black Si surfaces for photovoltaic applications. Effective integration of these anti-reflection surfaces into current devices will improve light collection efficacy. This will have important implications for future optoelectronic devices.

ACKNOWLEDGEMENTS

The authors would like to acknowledge financial support from the National Research Foundation, Prime Minister's Office, Singapore under its Competitive Research Program (CRP Award No. NRF-CRP10-2012-04) and the Economic Development Board (SPORE, COY-15-EWI-RCFSA/N197-1). The authors would also like to acknowledge funding provided by the Chinese Nature Science Grant (61138002) and 973 Program of China (No. 2013CBA01700).

1 Raut HK, Ganesh VA, Nair AS, Ramakrishna S. Anti-reflective coatings: a critical, in-depth review. *Energy Environ Sci* 2011; **4**: 3779–3804.
2 Fahim NF, Jia BH, Shi Z, Gu M. Simultaneous broadband light trapping and fill factor enhancement in crystalline silicon solar cells induced by Ag nanoparticles and nanoshells. *Opt Express* 2012; **20**: A694–A705.
3 Chen X, Jia BH, Saha JK, Cai B, Stokes N *et al*. Broadband enhancement in thin-film amorphous silicon solar cells enabled by nucleated silver nanoparticles. *Nano Lett* 2012; **12**: 2187–2192.
4 Zhang Y, Ouyang Z, Stokes N, Jia BH, Shi Z *et al*. Low cost and high performance Al nanoparticles for broadband light trapping in Si wafer solar cells. *Appl Phys Lett* 2012; **100**: 151101.
5 Yang L, Li X, Tuo X, Nguyen TT, Luo X *et al*. Alloy nanoparticle plasmon resonance for enhancing broadband antireflection of laser-textured silicon surfaces. *Opt Express* 2011; **19**: A657–A663.
6 Zhu J, Hsu CM, Yu ZF, Fan S, Cui Y. Nanodome solar cells with efficient light management and self-cleaning. *Nano Lett* 2010; **10**: 1979–1984.
7 Lee C, Bae SY, Mobasser S, Manohara H. A novel silicon nanotips antireflection surface for the micro Sun sensor. *Nano Lett* 2005; **5**: 2438–2442.
8 Li Y, Zhang J, Zhu S, Dong H, Jia F *et al*. Biomimetic surfaces for high-performance optics. *Adv Mater* 2009; **21**: 4731–4734.
9 Atwater HA, Polman A. Plasmonics for improved photovoltaic devices. *Nat Mater* 2010; **9**: 205–213.
10 Hou Y, Abrams BL, Vesborg PC, Björketun ME, Herbst K *et al*. Photoelectrocatalysis and electrocatalysis on silicon electrodes decorated with cubane-like clusters. *J Photonics Energy* 2012; **2**: 026001.
11 Zhmakin AI. Enhancement of light extraction from light emitting diodes. *Phys Rep* 2011; **498**: 189–241.

12 Chen HT, Zhou J, O'Hara JF, Chen F, Azad AK *et al*. Antireflection coating using metamaterials and identification of its mechanism. *Phys Rev Lett* 2010; **105**: 073901.
13 Xu L, Luo FF, Tan LS, Luo XG, Hong MH. Hybrid plasmonic structures: design and fabrication by laser means. *IEEE J Sel Top Quantum Electron* 2013; **19**: 4600309.
14 Vorobyev AY, Guo C. Antireflection effect of femtosecond laser-induced periodic surface structures on silicon. *Opt Express* 2011; **19**: A1031–A1036.
15 Vorobyev AY, Guo C. Direct creation of black silicon using femtosecond laser pulses. *Appl Surf Sci* 2011; **257**: 7291–7294.
16 Chattopadhyay S, Huang YF, Jen YJ, Ganguly A, Chen KH *et al*. Anti-reflecting and photonic nanostructures. *Mater Sci Eng R* 2010; **69**: 1–35.
17 Shen MY, Crouch CH, Carey JE, Mazur E. Femtosecond laser-induced formation of submicrometer spikes on silicon in water. *Appl Phys Lett* 2004; **85**: 5694–5696.
18 Liu Y, Hong MH. Ultralow broadband optical reflection of silicon nanostructured surfaces coupled with antireflection coating. *J Mater Sci* 2012; **47**: 1594–1597.
19 Liu Y, Liu S, Wang Y, Feng G, Zhu J *et al*. Broad band enhanced infrared light absorption of a femtosecond laser microstructured silicon. *Laser Phys* 2008; **18**: 1148–1152.
20 Spinelli P, Verschuuren MA, Polman A. Broadband omnidirectional antireflection coating based on subwavelength surface Mie resonators. *Nat Commun* 2012; **3**: 692.
21 Huang YF, Chattopadhyay S, Jen YJ, Peng CY, Liu TA *et al*. Improved broadband and quasi-omnidirectional anti-reflection properties with biomimetic silicon nanostructures. *Nat Nano* 2007; **2**: 770–774.
22 Kim KH, Park QH. Perfect anti-reflection from first principles. *Sci Rep* 2013; **3**: 1062.
23 Yang L, Feng Q, Ng B, Luo XG, Hong MH. Hybrid moth-eye structures for enhanced broadband antireflection characteristics. *Appl Phys Express* 2010; **3**: 102602.
24 Ma LL, Zhou YC, Jiang N, Lu X, Shao J *et al*. Wide-band ''black silicon'' based on porous silicon. *Appl Phys Lett* 2006; **88**: 171907.
25 Zhang S, Li Y, Feng G, Zhu B, Xiao S *et al*. Strong infrared absorber: surface-microstructured Au film replicated from black silicon. *Opt Express* 2011; **19**: 20462–20467.
26 Srivastava SK, Kumar D, Singh PK, Kar M, Kumar V *et al*. Excellent antireflection properties of vertical silicon nanowire arrays. *Sol Energy Mater Sol Cells* 2010; **94**: 1506–1511.
27 Striemer CC, Fauchet PM. Dynamic etching of silicon for broadband antireflection applications. *Appl Phys Lett* 2002; **81**: 2980–2982.
28 Sarnet T, Carey JE, Mazur E. From black silicon to photovoltaic cells, using short pulse lasers. *AIP Conf Proc* 2012; **1464**: 219–228.
29 Kumar D, Srivastava SK, Singh PK, Husain M, Kumar V. Fabrication of silicon nanowire arrays based solar cell with improved performance. *Sol Energy Mater Sol Cells* 2011; **95**: 215–218.
30 Garnett E, Yang P. Light trapping in silicon nanowire solar cells. *Nano Lett* 2010; **10**: 1082–1087.
31 Ding L, Wu QY, Song JF, Serita K, Tonouch M *et al*. Perfect broadband terahertz antireflection by deep-subwavelength thin lamellar metallic gratings. *Adv Opt Mater* 2013; **1**: 910–914.
32 Kim MJ, Na HJ, Lee KC, Yoo EA, Lee M. Preparation and characterization of Au–Ag and Au–Cu alloy nanoparticles in chloroform. *J Mater Chem* 2003; **13**: 1789–1792.
33 Dynich RA, Ponyavina AN. Effect of metallic nanoparticle sizes on the local field near their surface. *J Appl Spectrosc* 2008; **75**: 832–838.
34 Chong TC, Hong MH, Shi LP. Laser precision engineering: from microfabrication to nanoprocessing. *Laser Photon Rev* 2010; **4**: 123–143.
35 Srivastava SK, Kumar D, Singh PK, Kumar V. Silicon nanowire arrays based ''black silicon'' solar cells. In: Proceedings of the 34th IEEE Photovoltaic Specialists Conference 2009; 7–12 June 2009; Philadelphia, PA, USA. IEEE: Piscataway, NJ, USA, 2009, pp1851–1856.